MOLECULAR PHYSICS, 1996, VOL. 88, NO. 3, 821–840

Use of simulated infrared spectra to test N_2–Ar pair potentials and dipole moment surfaces

By FENG WANG, FREDERICK R. W. McCOURT and ROBERT J. LE ROY
Guelph–Waterloo Center for Graduate Work in Chemistry, University of Waterloo, Waterloo, Ontario N2L 3G1, Canada

(*Received 17 October 1995; accepted 21 January 1996*)

Infrared spectra of the $^{14}N_2$–Ar van der Waals complex have been simulated by performing exact quantum mechanical calculations using two recent potential energy surfaces, one having a modified Morse–Morse–spline–van der Waals form and the other an exchange-Coulomb (XC) model form. Frequencies and intensities have been calculated for some 10^5 spectral transitions amongst the bound states of the complex, and simulations of the mid-infrared (2290–2370 cm^{-1}) spectrum of the complex at 77 K constructed from superpositions of lines, each of which has been assigned a Lorentzian lineshape with a linewidth appropriate to the experimental conditions. The roles of the various terms in the effective dipole moment surface proposed by Ayllón *et al.* (1990, *Molecular Physics*, **71**, 1043) have also been examined, and a modification made which yields improved agreement with the experimental mid-infrared spectrum obtained by McKellar (1988, *Journal of Chemical Physics*, **88**, 4190). Based upon the present calculations, the 48 most intense bands of the simulated spectrum of the $^{14}N_2$–Ar van der Waals complex have been given vibrational assignments. The spectrum simulated from the modified Morse-type potential surface, when employed together with the present modified dipole moment surface, shows distinctly better agreement with experiment than does the spectrum simulated from either the XC or the earlier empirical potential energy surface. Far-infrared spectra have also been simulated at 5 K and at 77 K using an appropriate effective dipole surface, and compared with the calculation of Ayllón *et al.*

1. Introduction

The N_2–Ar interaction has been untilized as a prototype system in the development of methods for the empirical determination of anisotropic potential energy surfaces for atom–(heavy rotor) species [1–8]. Until very recently, most of the information used in such determinations consisted of scattering cross-sections and a variety of bulk property measurements, and the model dependence and uncertainties arising from the partial wave and apparatus or thermal averaging associated with those properties had left a considerable amount of ambiguity. The microwave data recently reported for N_2–Ar have now very sharply defined the radial position and shape of this potential near its minimum [7, 9]. However, there remains considerable uncertainty regarding its radial and angular behaviour at higher energies.

High resolution infrared (IR) spectra of weakly bound van der Waals complexes are perhaps the best single source of information about intermolecular potentials, since the transition frequencies and intensities directly reflect the energies and wavefunctions of individual states, and the range of levels observable in the infrared spans essentially the entire attractive potential well. However, although N_2–Ar was one of the first heavy rotor complexes for which discrete infrared spectra were observed [10], even the most recent of such studies [11] has not yet attained rotational

0026–8976/96 $12·00

resolution. In particular, McKellar's recent IR spectrum for this system [11] does show considerable structure, at least some of which may be assignable to individual vibrational bands. However, its interpretation is complicated by the fact that each observed peak is a sum of many individual transitions, and hence depends not only upon the intensities but also upon the pattern and densities of the individual lines [12, 13]. While the line positions depend only upon the accuracy of the potential energy surface, the line intensities depend upon both the potential and dipole moment surfaces. Since both are at least partly unknown, and the simulation of the unresolved IR spectrum is computationally very demanding (see below), it is difficult to use such spectra directly in the empirical determination of a potential energy surface. However, it is certainly possible to use simulated IR spectra to test available potential surfaces, and possibly also to improve the model dipole moment surfaces.

Simulation of intensities in the IR spectra of van der Waals complexes can be tedious and computationally expensive, and only a few authors have examined the intensities as well as the patterns of transition frequencies in such systems [12–18]. If the spectra are not fully resolved, all possible allowed transitions among thermally accessible bound states must be calculated and merged together with finite-width lineshape functions to allow meaningful comparisons with experiment. For a very weakly bound complex such as He–CO, which has a total of only 13 bound states, the number (108) of such transitions is modest and the calculations are not overly demanding [18]. However, for a complex with a larger reduced mass and a deeper potential well, the situation is quite different. For example, the N_2–Ar potentials employed here support some 2000 bound states, and the synthetic IR spectrum consists of a total of around 10^5 discrete allowed transitions, so that its simulation using high accuracy quantal calculations becomes quite time-consuming.

In spite of this difficulty, the IR spectrum of the N_2–Ar complex has attracted considerable theoretical attention. In 1982, Beswick and Shapiro [14] reported exact close coupling calculations of the lineshapes of IR transitions involving rotationally predissociating levels of this complex, using relatively simple potential energy and dipole moment surfaces. More recently, Brocks and van der Avoird [16, 17] simulated the overall bound $\rightarrow$ bound portion of the N_2–Ar spectrum using the empirically determined potential surface of Candori *et al.* [3] (identified henceforth as the CPV potential). However, their calculations considered only the lowest rotational states of the complex and did not take account of Coriolis coupling. Moreover, in the absence of a reliable dipole moment function, they assumed that all transitions allowed by a chosen set of approximate selection rules had the same intensity [16, 17].

The first comprehensive and realistic simulations of the N_2–Ar IR spectrum were those reported by Ayllón *et al.* [13] who combined a full semi-empirical model for the dipole moment surface with the same CPV potential surface [3] used by Brocks and van der Avoird. They used an essentially exact quantum treatment of the dynamics of the complex in their calculations, and included all possible transitions amongst *all* bound vibration–rotation levels of the system, so that comparisons with experiment could provide a quantitative test of the potential and dipole surfaces used. Unfortunately, while their simulated spectra showed structure analogous to that seen experimentally, there was only modest similarity. Thus, even with the limited resolution currently available, the IR data seem to provide a rather discerning test of the available surfaces.

Since the work of Ayllón *et al.* [13] an improved anisotropic N_2–Ar potential energy surface has been obtained by Beneventi *et al.* [6] from a multiproperty fit to

total differential and integral scattering cross-sections and a variety of macroscopic properties. It has a 'Morse–Morse–Spline–van der Waals' (MMSV) form, and its agreement with all available gas-phase data for this system has been shown to be distinctly better than that obtained with the CPV surface [6]. This potential was further refined by Jäger *et al.* [7] (yielding a surface-labeled $MMSV_{mod}$), who also required it to agree with their new microwave data for this species. In addition, a theoretically based exchange-Coulomb (XC) model potential energy surface (labelled XC-3) has very recently been proposed by Dham *et al.* [8]. The objectives of the present work were therefore twofold: (i) to compare the simulated mid-IR spectrum obtained from these new potential energy surfaces with the experimental IR spectrum obtained by McKellar [11]; and (ii) to understand better the roles of the various terms that contribute to the dipole moment surface.

Two separate sets of simulations have been carried out for this study: in the first, the mid-IR spectrum of the N_2–Ar complex has been generated for the experimental temperature and total pressure using the $MMSV_{mod}$ potential surface and the dipole moment functional form given in [13]. Parameters governing the short and long range contributions to the transition dipole surface were then varied in an attempt to obtain a simulated spectrum that better matched the experimental one, and simulations carried out using both the $MMSV_{mod}$ and XC-3 potential energy surfaces. In the second set of simulations, a dipole moment surface for far-IR transitions was constructed from *ab initio* values for the N_2 quadrupole and hexadecapole moments [19], and used to predict the far-IR spectrum of the complex. The potential energy surfaces utilized in this study and the bound states supported by them are discussed in section 2. Section 3 describes the forms of dipole moment surface utilized for the intensity calculations, while the computational methodology is outlined in section 4. Results for the mid-IR spectrum of the $^{14}N_2$–Ar complex are then presented in section 5, and predictions for the far-IR spectrum in section 6. Finally, conclusions drawn from the present study are given in section 7.

2. Potential energy surfaces and bound states

The potential energy surfaces currently available for the N_2–Ar complex depend upon the distance $R = |\mathbf{R}|$ separating the monomer centres-of-mass and the angle θ between $\hat{\mathbf{R}} \equiv \mathbf{R}/R$ and the N_2 figure axis; in particular, they do *not* depend on the monomer stretching coordinate r. These two-dimensional potential surfaces have the bond length of the N_2 monomer fixed at the equilibrium distance r_0 for its $v = 0$ ground vibrational state. For the van der Waals complex, R thus serves as the stretching coordinate and θ as a bending coordinate.

Values of the position and depth of the minimum in the interaction energy between a homonuclear diatomic molecule and an atom at the linear and T-shaped geometries are often used to characterize the anisotropy of the surface. It is also useful to consider a third representative quantity, the position σ at which the potential energy changes sign in each of these configurations. These features of the CPV, $MMSV_{mod}$ and XC-3 potential energy surfaces are given in table 1, together with their differences for the two orientations. For all three potential surfaces the most stable structure has a T-shaped geometry. Figure 1 compares one-dimensional cuts through the CPV, $MMSV_{mod}$ and XC-3 potential surfaces for $\theta = 90°$ (T-shaped structure) and $\theta = 0°$ (linear structure). For the T-shaped geometry, the minima of both the $MMSV_{mod}$ and XC-3 potential surfaces are shifted approximately 0·15 Å further out than that for the CPV surface,

Table 1. Potential energy surface characteristics.

Properties[a]	CPV	$MMSV_{mod}$	XC-3
$\varepsilon_{\|}/cm^{-1}$	70·98	60·82	56·87
$\varepsilon_{\perp}/cm^{-1}$	103·24	106·47	102·52
$\Delta\varepsilon/cm^{-1}$	32·26	45·65	45·65
$R_{m\|}/Å$	3·96	4·33	4·37
$R_{m\perp}/Å$	3·57	3·70	3·73
$\Delta R_m/Å$	−0·39	−0·63	−0·64
$\sigma_{\|}/Å$	3·55	3·84	3·90
$\sigma_{\perp}/Å$	3·20	3·30	3·29
$\Delta\sigma/Å$	−0·35	−0·54	−0·61

[a] $\Delta Q \equiv Q_{\perp} - Q_{\|}$.

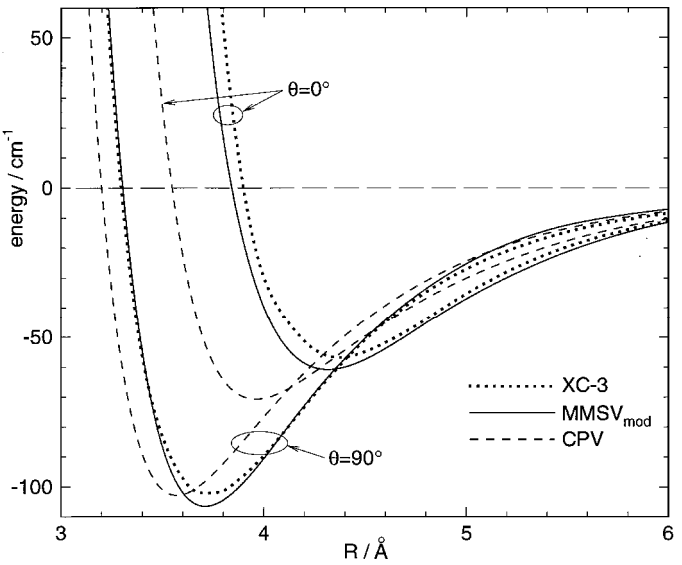

Figure 1. Cuts through the CPV, $MMSV_{mod}$ and XC-3 potential energy surfaces for N_2–Ar at $\theta = 0°$ and $\theta = 90°$.

with the $MMSV_{mod}$ minimum being slightly deeper and the XC-3 minimum slightly shallower than that for the CPV surface. For the linear geometry, the $MMSV_{mod}$ and XC-3 surfaces both have minima that are shifted outwards by approximately 0·35 Å relative to that for the CPV surface, and both wells are significantly shallower than that for the CPV surface. Compared to the $MMSV_{mod}$ surface, the XC-3 potential has slightly shallower wells for both the T-shaped and linear geometries.

Pure vibrational states (those for which $J = 0$) and transitions amongst them can be assigned in terms of the approximate quantum numbers v_s and v_b representing the numbers of nodes of the vibrational wavefunction in the stretching coordinate R and in the bending coordinate θ, respectively [17]. Moreover, the vibrationally assigned energy levels can be further grouped into two symmetry assignments [10, 17], since even bending states have s symmetry, and odd bending states have a symmetry (corresponding to *ortho*- and *para*-N_2, respectively). The threshold energy below

Table 2. Assignments[a] for the 48 most intense vibrational transitions ($v' = 1$, $v'' = 0$, $J' = J'' = 0$) of the $^{14}N_2$–Ar complex.

(v'_s, v'_b)	(v''_s, v''_b)	ν/cm^{-1}	(v'_s, v'_b)	(v''_s, v''_b)	ν/cm^{-1}
0,2	4,0	2292·962	1,4	1,4	2329·500
0,0	0,2	2295·172	4,0	4,0	2329·500
0,1	0,3	2295·764	2,2	2,2	2329·500
0,2	3,0	2298·688	3,0	3,0	2329·500
0,3	3,1	2309·601	0,4	0,4	2329·500
1,1	0,3	2312·850	1,2	1,2	2329·500
2,1	1,3	2315·832	2,0	2,0	2329·500
1,2	3,0	2316·842	0,2	0,2	2329·500
1,0	0,2	2317·767	1,0	1,0	2329·500
2,0	1,2	2318·689	0,0	0,0	2329·500
0,4	3,0	2320·937	5,1	4,1	2331·555
2,2	1,4	2322·781	4,1	0,5	2335·453
0,5	4,1	2323·547	1,4	2,2	2336·219
4,1	5,1	2327·445	3,0	0,4	2338·063
5,1	5,1	2329·500	0,5	1,3	2339·837
4,1	4,1	2329·500	1,2	2,0	2340·311
0,5	0,5	2329·500	3,0	1,2	2342·158
3,1	3,1	2329·500	1,3	2,1	2343·168
1,3	1,3	2329·500	0,3	1,1	2346·150
2,1	2,1	2329·500	3,1	0,3	2349·399
0,3	0,3	2329·500	3,0	0,2	2360·312
1,1	1,1	2329·500	0,3	0,1	2363·236
0,1	0,1	2329·500	0,2	0,0	2363·828
5,0	5,0	2329·500	4,0	0,2	2366·038

[a] Based on calculations using the $MMSV_{mod}$ potential surface.

which states of the N_2–Ar complex are truly bound is the energy of the lowest total parity-allowed dissociation channel, i.e. $E(j_{N_2} = 0) = 0{\cdot}0$ cm^{-1} or $E(j_{N_2} = 1) = 3{\cdot}98$ cm^{-1}. All three potential surfaces considered here have 22 bound vibrational states, of which 12 have *s* symmetry and 10 have *a* symmetry. Since only $s \rightarrow s$ and $a \rightarrow a$ transitions are allowed, these 22 bound levels give rise to 244 possible allowed mid-IR vibrational transitions, which can be used to attempt a vibrational assignment of the simulated and experimental IR spectra. Table 2 lists the 48 most intense vibrational transitions for a temperature of 77 K, as calculated from the $MMSV_{mod}$ potential surface.

For the CPV potential surface the ground vibrational state of the $^{14}N_2$–Ar complex is bound by 77·99 cm^{-1}, while the corresponding values obtained for the $MMSV_{mod}$ and XC-3 potential surfaces are 81·34 and 81·96 cm^{-1}, respectively. The present result for the CPV surface differs slightly from the value 77·96 cm^{-1} obtained earlier by Ayllón *et al.* [13] because of our use of updated physical constants [20]. All 22 bound pure vibrational energy levels generated using the three potential surfaces are shown in figure 2. A common pattern is found for the bound vibrational levels of the $MMSV_{mod}$ and XC-3 potential surfaces, with the vibrational energy levels for each being shifted relative to those calculated from the CPV potential surface.

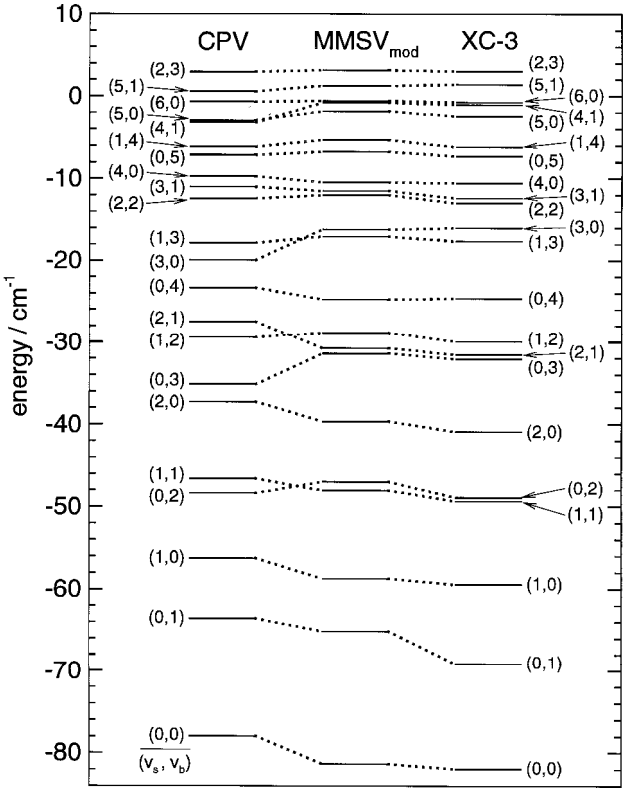

Figure 2. Energy levels for the pure vibrational modes of the N_2–Ar van der Waals complex, as determined from the CPV, MMSV$_{mod}$ and XC-3 potential energy surfaces.

3. Dipole moment surfaces

The dipole moment surfaces governing far-IR and mid-IR spectral transitions differ both in the sets of values for the parameters which characterize them and in their radial behaviour. The dipole moment is a vector function which, for an atom–diatom van der Waals complex, can be denoted $\mu(\mathbf{R}, \mathbf{r})$; $\mathbf{R}$ has been defined above, and the vector $\mathbf{r} \equiv r\hat{\mathbf{r}}$ joins nuclei of the diatom. The N_2–Ar van der Waals complex is assumed to lie in the xz-plane with the body-fixed coordinate system located at the centre-of-mass of the complex and the z-axis lying along $\hat{\mathbf{R}}$.

There are three common sources for a dipole moment surface: (i) permanent dipole moments of the constituent monomers; (ii) dipole moments induced in one monomer by the electric field associated with a non-spherical charge distribution in the other; and (iii) distortion of the electronic structure of the monomers owing to electron overlap or charge transfer [21]. Dipole surfaces for most van der Waals complexes in their ground electronic states are determined predominantly by the first two sources, while the third tends to become important at short range. In the present case the first source is absent, since the N_2 molecule has no permanent dipole moment; the leading induction contributions to the dipole surface are due to the interaction of the permanent quadrupole and hexadecapole moments of N_2 with the polarizability of Ar.

Infrared transitions of the N_2–Ar complex in general involve changes in both the van der Waals and monomer (N_2) vibration–rotation states. Because the vibration–

rotation states of the complex are so much more closely spaced than those of N_2, the van der Waals transitions are clustered around central frequencies corresponding to the $v' \leftarrow v''$ N_2 vibrational transitions, where v'' and v' are the initial and final vibrational quantum numbers for N_2. We are interested specifically in two absorption bands, one in the far-IR, attributable to pure van der Waals transitions in which the N_2 monomer remains in its ground vibrational state (i.e. $v' = v'' = 0$), the other in the mid-IR attributable to simultaneous van der Waals and $v'' = 0 \rightarrow v' = 1$ transitions of N_2.

The Cartesian components of the leading induction and dispersion contributions to the dipole surface responsible for the far-IR spectrum of the N_2–Ar complex have been given by Ayllón *et al.* [13] as

$$\mu_z^{00}(R, \theta) = \frac{D_7^{00}}{R^7} P_0^0(\cos\theta) + \left(\frac{9}{5}\right)^{1/2} \frac{Q^{00}\alpha}{R^4} P_2^0(\cos\theta) + \frac{5}{3}\frac{\Phi^{00}\alpha}{R^6} P_4^0(\cos\theta) \quad (1)$$

$$\mu_x^{00}(R, \theta) = -\left(\frac{3}{5}\right)^{1/2} \frac{Q^{00}\alpha}{R^4} P_2^1(\cos\theta) - \left(\frac{10}{9}\right)^{1/2} \frac{\Phi^{00}\alpha}{R^6} P_4^1(\cos\theta), \quad (2)$$

in which D_7^{00}, Q^{00} and Φ^{00} are, respectively, vibrationally-averaged values of the dipole dispersion coefficient, $D_7(r)$, and of the permanent quadrupole and hexadecapole moments, $Q(r)$ and $\Phi(r)$, for the N_2 molecule in its ground vibrational state, while α is the polarizability of the Ar atom.

The mid-IR spectrum of the complex will be centered around the effective monomer fundamental stretch frequency, located at 2329·50 cm^{-1} [11]. The dipole surface governing mid-IR transitions is determined by a set of expansion coefficients similar in structure to those responsible for the far-IR transitions. If the r-dependences of Q, Φ and D_7 are expanded in Taylor series about the equilibrium distance r_e of the N_2 monomer, then the leading long-range components of the dipole surface governing the mid-IR spectrum of the complex can be written as [13, 15]:

$$\mu_z^{10}(R, \theta) = \langle 1|\Delta r|0\rangle \left[\frac{D_7'}{R^7} P_0^0(\cos\theta) + \left(\frac{9}{5}\right)^{1/2} \frac{Q'\alpha}{R^4} P_2^0(\cos\theta) + \frac{5}{3}\cdot\frac{\Phi'\alpha}{R^6} P_4^0(\cos\theta)\right], \quad (3)$$

$$\mu_x^{10}(R, \theta) = \langle 1|\Delta r|0\rangle \left[-\left(\frac{3}{5}\right)^{1/2} \frac{Q'\alpha}{R^4} P_2^1(\cos\theta) - \left(\frac{10}{9}\right)^{1/2} \frac{\Phi'\alpha}{R^6} P_4^1(\cos\theta)\right], \quad (4)$$

in which $\langle 1|\Delta r|0\rangle \equiv \langle v' = 1|r - r_e|v'' = 0\rangle$, while D_7', Q' and Φ' are the first derivatives of $D_7(r)$, $Q(r)$ and $\Phi(r)$ with respect to the diatom bond length r, evaluated at r_e. *Ab initio* values for the derivatives Q' and Φ' for the N_2 molecule have been obtained by Amos [22]. The present study focuses upon the role of the dominant contributions to the dipole moment surface given in [13], and how they influence the simulated mid-IR spectrum of the N_2–Ar complex. Work is currently underway on producing optimum dipole moment surfaces for both far- and mid-IR simulations.

Although the vibrational matrix element $\langle 1|\Delta r|0\rangle$ of the N_2 monomer appearing in equations (3) and (4) may be evaluated using the harmonic oscillator (HO) approximation, a more accurate value can readily be obtained for a realistic intramolecular potential function. In the HO limit $\langle 1|\Delta r|0\rangle^{HO}$ is given as $(h/8\pi^2\mu\bar{\nu}c)^{1/2}$, with h Planck's constant, c the speed of light, and μ and $\bar{\nu}$ the appropriate reduced mass and fundamental oscillator frequency. For N_2, with μ = 7·0 amu and $\bar{\nu}$ = 2330·0 cm^{-1}, $\langle 1|\Delta r|0\rangle^{HO}$ has the value 0·060 753 a_0, while a numerical evaluation using a

Rydberg–Klein–Rees N_2 intramolecular potential based upon parameters taken from Huber and Herzberg [23] gives the value $\langle 1|\Delta r|0\rangle = 0{\cdot}060\,556\ a_0$. The latter value is employed in the present calculations.

4. The calculations

The far-IR and mid-IR spectra of N_2–Ar can be simulated for any assumed potential energy surface once appropriate dipole moment surfaces have been obtained. The dipole moment surface $\mu(\mathbf{r}, \mathbf{R})$ of a van der Waals complex may be expanded using the same type of orthonormal body-fixed angular momentum basis functions used to characterize the rotational motion. As the total parity of the wavefunction must change in an electric dipole-allowed transition, the transition dipole matrix elements are subject to the usual selection rules

$$\Delta J = 0, \quad \Delta p = \pm 1 \tag{5}$$

and

$$\Delta J = \pm 1, \quad \Delta p = 0, \tag{6}$$

in which $p = 0$ or 1 is the e/f parity quantum number, defined such that the total parity of the complex is given by $(-1)^{J+p}$ [21, 24].

A typical spectral simulation is performed in the following way. The first step involves calculation of the eigenvalues and eigenfunctions of all bound states of the complex and the computation of the associated transition intensities or line strengths, $S(\mathrm{f} \leftarrow \mathrm{i})$, for all possible combinations of initial and final states. Since the potential energy surfaces used do not depend upon the rovibrational state of the component N_2 molecule, the total upper state energies E_f for the mid-IR spectra are obtained simply by adding the observed vibrational band energy [11] $\nu_0 = 2329{\cdot}50\ \mathrm{cm}^{-1}$ to the directly calculated level energies. The second step of the simulation involves the assignment to each transition of a thermal weight factor to give the final integrated absorption intensity at temperature T, namely [13, 25]

$$I(\nu_{\mathrm{if}}) = \frac{8\pi^3 \nu_{\mathrm{if}} g_\mathrm{i} [\exp(-E^\mathrm{i}/k_\mathrm{B}T) - \exp(-E^\mathrm{f}/k_\mathrm{B}T)]}{3hcQ(T)} S(\mathrm{f} \leftarrow \mathrm{i}), \tag{7}$$

in which $\nu_{\mathrm{if}} \equiv E^\mathrm{f} - E^\mathrm{i}$ is the transition frequency of the complex, g_i is the nuclear-spin degeneracy of the initial state, $Q(T)$ is the canonical partition function (a function of temperature only), while k_B is the Boltzmann constant. The intensity factor can be rewritten in the form

$$I(\nu_{\mathrm{if}}) = F(\nu_{\mathrm{if}}, T)\, W_{\mathrm{if}}, \tag{8}$$

with $W_{\mathrm{if}} \equiv 8\pi^3 g_\mathrm{i} \mathrm{e}^{-E^\mathrm{i}/k_\mathrm{B}T} S(\mathrm{f} \leftarrow \mathrm{i})/[3hcQ(T)]$ and $F(\nu_{\mathrm{if}}, T) = \nu_{\mathrm{if}}[1 - \exp(-\nu_{\mathrm{if}}/k_\mathrm{B}T)]$. For the far-IR spectrum the factor $F(\nu_{\mathrm{if}}, T)$ tends to discriminate strongly against low-frequency transitions, while for transitions appearing in the mid-IR spectrum it is a weakly varying function of frequency, because a range of about $80\ \mathrm{cm}^{-1}$ around ν_0 does not represent a significant variation of ν_{if}.

Calculation of the integrated intensities for the allowed transitions via step two results in a stick spectrum. In the third step, the overall spectral profile is generated from the stick spectrum by assigning a characteristic lineshape, representing the type of line broadening appropriate to a bulk gas spectrum at the experimental temperature and pressure, and summing up the contributions from the full set of broadened lines.

Since the potential surfaces considered do not depend upon the internal rovibrational state of the N_2 monomer, any asymmetry obtained for the mid-IR spectrum is due to thermal weighting and modest changes in the temperature-dependent frequency factor which weights the various spectral lines.

Simulation of the full experimental spectral profile requires a knowledge of all individual line positions and line strengths. The present calculations include all truly bound states. For both the $MMSV_{mod}$ and XC-3 potentials, this includes the range $0 \leqslant J_{tot} \leqslant 34$; this upper bound is only slightly larger than that for the CPV potential, namely $J_{tot}(max) = 32$ [13]. Although experimental spectra were recorded at a number of temperatures ranging from 77 to 87 K [11], the structure is most clearly resolved at the lowest temperature (77 K), for which most of the simulations reported here have been performed. The linewidths were assumed to be dominated by collision broadening, and were all represented by Lorentzian lineshape functions with a common width parameter: following [13], the value 0·20 cm^{-1} was used to accord with McKellar's experimental conditions (T = 77 K, total density = 1·7 amagat) [11].

For each potential energy surface considered, the bound vibration–rotation eigenstates have been determined for the $^{14}N_2$–Ar isotopomer using the TRIATOM program suite of Tennyson *et al.* [25], which is the same (variational) procedure used by Ayllón *et al.* [13]. Atom–diatom scattering coordinates were used, and the $^{14}N_2$ monomer bond length was fixed at a value of 2·078 836 665 a_0, which corresponds to the experimental [26] inertial rotational constant B_0 for the free $^{14}N_2$ monomer (cf. the value 2·0667 a_0 employed by Ayllón *et al.* [13]). As in previous work [7], the radial basis set consists of 40 Morse-oscillator-like functions defined by the Morse function parameters $R_e = 11{\cdot}6\ a_0$, $D_e = 8{\cdot}5 \times 10^{-5} E_h$ and $\omega_e = 2{\cdot}2 \times 10^{-5} E_h$. These values differ slightly from the parameters used by Ayllón *et al.* [13], but the change has no significant effect on the calculated results. Updated physical constants [20] have been employed in these calculations, and the masses for Ar and ^{14}N have been taken to be $m(Ar)$ = 39·962 3837 amu and $m(^{14}N)$ = 14·003 074 002 amu.

5. Mid-infrared spectral simulations

5.1. *Simulations based upon empirical model dipole surfaces*

The model dipole surface utilized in our first simulation of the mid-IR spectrum was that of [13], namely

$$\mu_z^{10}(R,\theta) = \langle 1|\Delta r|0\rangle \left\{ \left(D'_{01} e^{-(R-\sigma)/\rho} + \frac{D'_7}{R^7} \right) P_0^0(\cos\theta) + \left[\left(\frac{3}{5}\right)^{1/2} D'_{23} e^{-(R-\sigma)/\rho} + \left(\frac{9}{5}\right)^{1/2} \frac{Q'\alpha}{R^4} \right] P_2^0(\cos\theta) + \frac{5}{3}\frac{\Phi'\alpha}{R^6} P_4^0(\cos\theta) \right\}, \quad (9)$$

$$\mu_x^{10}(R,\theta) = -\langle 1|\Delta r|0\rangle \left\{ \left[\left(\frac{1}{5}\right)^{1/2} D'_{23} e^{-(R-\sigma)/\rho} + \left(\frac{3}{5}\right)^{1/2} \frac{Q'\alpha}{R^4} \right] P_2^1(\cos\theta) + \left(\frac{10}{9}\right)^{1/2} \frac{\Phi'\alpha}{R^6} P_4^1(\cos\theta) \right\}. \quad (10)$$

The quantities σ and ρ characterize the size of the complex and the range of the interaction, while D'_{01}, D'_{23} and D'_7 are all empirical parameters, the first two representing the overlap contributions and the last one the isotropic dispersion contribution to the dipole moment surface. Specifically, [13] used values 0·0698$e\,a_0^2$

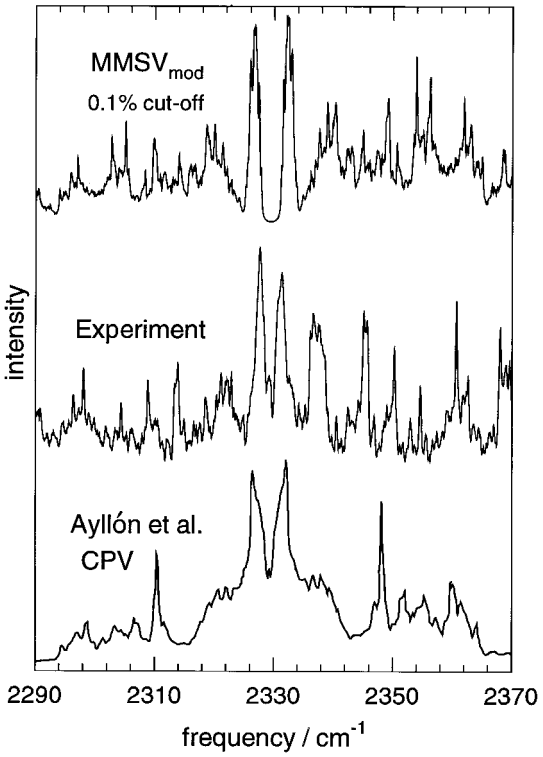

Figure 3. Comparisons between experiment [11] and simulated 77 K mid-IR spectra generated using the MMSV$_{mod}$ and CPV potential energy surfaces; both simulations used the 0·1% intensity cut-off criterion and dipole surface of Ayllón *et al.* [13].

and $0{\cdot}153e\,a_0^4$ for the products $Q'\langle 1|\Delta r|0\rangle$ and $\Phi'\langle 1|\Delta r|0\rangle$,† while values for the other parameters were $\alpha(\mathrm{Ar}) = 11{\cdot}075\,a_0^3$, $\sigma = 6{\cdot}5\,a_0$ and $\rho = 0{\cdot}11\sigma$. The derivatives D'_{01} and D'_{23} of the overlap parameters and D'_7 of the dispersion dipole parameter were determined empirically, in an effort to obtain the best simulation of the experimental spectrum, using the CPV potential surface. The dipole surface obtained in this manner in [13] will be referred to henceforth as the DIP-0 surface.

Figure 3 compares the synthetic mid-IR spectrum of the $^{14}N_2$–Ar complex at 77 K generated from the MMSV$_{mod}$ surface, both with the experimental results of McKellar [11] and with the spectrum generated from the CPV potential surface by Ayllón *et al.* [13]. Following [13] and [27], this initial mid-IR spectrum was obtained while neglecting all transitions with intensities less than 0·1% of the most intense line. The spectrum thus generated from the MMSV$_{mod}$ surface shows modest agreement with experiment, agreement which is distinctly better than that yielded by the CPV surface. However, we found that the 0·1% intensity cut-off makes a significant difference in the calculation of the mid-IR spectrum, particularly in the region near the band centre. The effect of this cut-off is demonstrated in figure 4, which compares simulated mid-IR spectra obtained with and without this 0·1% intensity cut-off. The central peaks of

† Ayllón *et al.* list values of $0{\cdot}0698e\,a_0$ and $0{\cdot}153e\,a_0^3$ for Q' and Φ' in their table 2: these numerical values actually correspond to $Q'\langle 1|\Delta r|0\rangle^{HO}$ and $|\Phi'|\langle 1|\Delta r|0\rangle^{HO}$, with Q' and $|\Phi'|$ having their *ab initio* values.

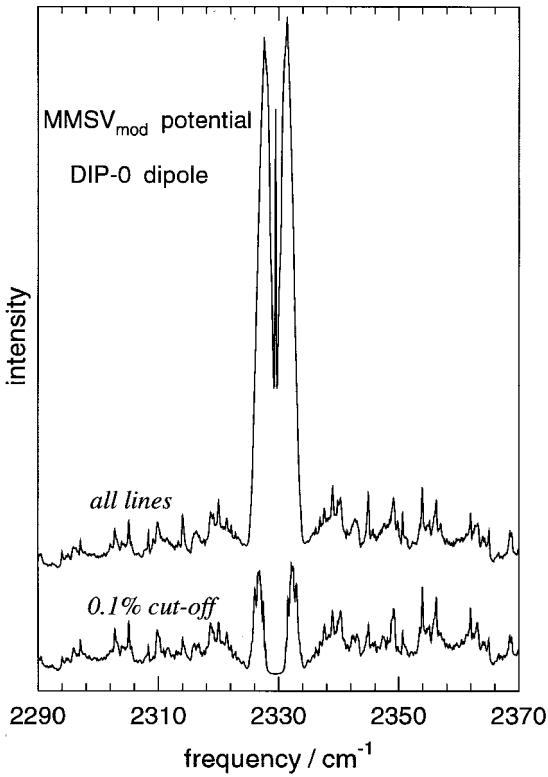

Figure 4. Comparison of mid-IR spectra simulated at 77 K for 0·2 cm^{-1} Lorentzian linewidths using the MMSV$_{mod}$ potential surface and the dipole surface of Ayllón *et al.* [13], with and without employment of a 0·1% intensity cut-off criterion.

the full spectrum are clearly much stronger when this cut-off criterion is not applied. More generally, we found that application of a cut-off criterion which neglects all transitions with intensities 10^{-3}, 10^{-6}, 10^{-9} or 10^{-12} smaller than that of the most intense line deleted, respectively, 52·6, 9·3, 1·4 or 0·19% of the calculated transitions. Thus, the 0·1% intensity cut-off criterion introduced in [13] neglects roughly one half of the transitions contributing to the spectrum. While superficially plausible, figure 4 shows that this cut-off criterion yields unacceptable results, and that the mid-IR spectral simulations should include all possible transitions, particularly in the band-centre region. No cut-off criterion is employed in subsequent simulations.

The full mid-IR spectrum simulated using the MMSV$_{mod}$ potential and the DIP-0 dipole gives reasonably qualitative agreement with experiment [11], except in the neighbourhood of the band centre. This suggests that some modifications of the effective dipole moment surface are required, since some of its parameters, such as that associated with the dispersion induced-dipole, D_7', and the overlap parameters, D_{01}' and D_{23}', were determined empirically on the basis of calculations made with the CPV potential surface and the 0·1% intensity cut-off criterion [13]. The parameters of equations (9) and (10) defining the various modified dipole moment surfaces considered below are summarized in table 3.

Qualitative arguments along the lines presented by Chuaqui *et al.* [18] suggest that the isotropic component of the dipole moment surface contributes mainly to the

Table 3. Parameters characterizing the effective dipole moment functions of equations (9) and (10) used in the mid-IR spectra simulations.

Model surface	$D'_{23}/10^{-4}e$	$D'_{01}/10^{-4}e$	$D'_7/10^3 e\,a_7^7$	$Q'/e\,a_0$	$\Phi'/e\,a_0^3$
DIP-0 [a,b]	64·2	42·8	4·28	1·15	2·52
DIP-1 [b]	64·2	42·8	1·91	1·15	2·52
DIP-2 [b]	0·0	0·0	1·91	1·15	2·52
DIP-3 [b]	64·2	19·1	−1·91	1·15	2·52
DIP-4 [c]	0·0	0·0	0·0	1·15	−2·53

[a] Dipole surface given in [13].
[b] The additional parameters defining these dipole surfaces are $\alpha = 11{\cdot}075\ e\,a_0^3$, $\sigma = 6{\cdot}5a_0$ and $\rho = 0{\cdot}11\sigma$, as in [13].
[c] Improved model dipole surface using $\alpha = 11{\cdot}062a_0^3$ from [19].

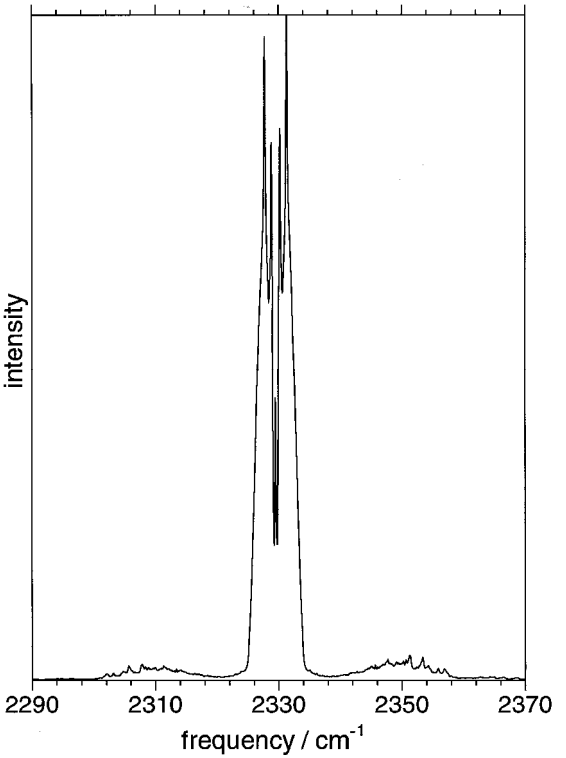

Figure 5. Mid-IR spectrum at 77 K for 0·2 cm^{-1} Lorentzian linewidths simulated using the $MMSV_{mod}$ potential surface and a model dipole surface consisting only of the isotropic dispersion term.

central peaks in the mid-IR spectrum. In order to test this hypothesis, we performed a simulation of the mid-IR spectrum in which the dipole moment surface consisted of only the isotropic dispersion term $\langle 1|\Delta r|0\rangle D'_7 P_0^0(\cos\theta)\, R^{-7}$. The resulting spectrum, shown in figure 5, demonstrates that this term indeed contributes almost solely to the central peak region. It is also interesting to note that (using the DIP-0 D'_7 value from table 3) the highest peak in this spectrum is 50% more intense than that in the spectrum obtained using the full DIP-0 surface. Because this value for $\langle 1|\Delta r|0\rangle D'_7$ was

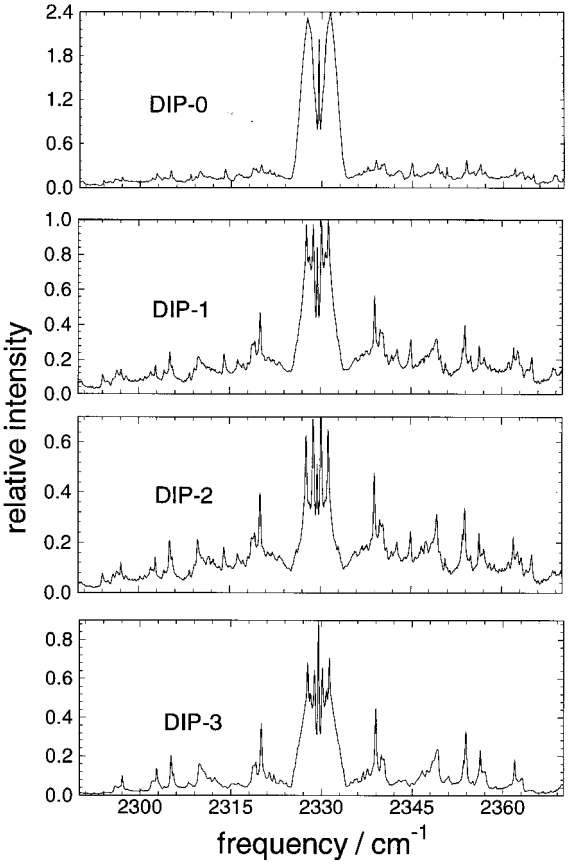

Figure 6. Mid-IR spectra at 77 K for 0·2 cm^{-1} Lorentzian linewidths simulated using the MMSV$_{mod}$ potential and dipole moment surfaces DIP-0 through DIP-3 (see equations (9) and (10), and table 3).

determined in [13] from simulations in which a 0·1% cut-off criterion was employed, and these peaks in our simulation using the MMSV$_{mod}$ potential surface are about five-times stronger than they should be (see figure 4), it seemed reasonable to reduce the value assumed for D_7' by $\sqrt{5}$. The dipole surface so obtained is designated DIP-1.

Figure 6 shows that the DIP-1 dipole surface yields much more realistic overall central peak intensities than did the original DIP-0 surface of [13] (cf. figure 3). However, it also gives a much higher degree of structure in this central region than was observed experimentally. In an attempt to eliminate this spurious structure, we examined the effects of further empirical changes to the nature of the dipole moment surface. In particular, calculations were performed for dipole DIP-2 which has no short-range contributions (i.e., for which $D_{01}' = D_{23}' = 0$), as well as for one (DIP-3) with a modified D_{01}' value and for which the sign of D_7' was reversed (see table 3). The resulting 77K mid-IR spectra are shown in figure 6, in which all plots are normalized relative to the most intense peak of the DIP-1 simulation. Although the relative intensities of the central peaks in spectra obtained using the DIP-1 through DIP-3 dipole surfaces are all much closer to experiment than those for the original DIP-0 surface, none of these dipole models produces a mid-IR spectrum with unstructured central peaks.

Some idea of the relative importance of the various contributions to the dipole surface can be gleaned from comparisons amongst these simulated spectra. For example, comparison of the DIP-2 and DIP-1 spectra indicates that neglecting the short-range contributions to the dipole surface reduces both the overall intensity of the simulated spectrum and the relative importance of the central peaks. Similarly, comparison of the spectra simulated using the DIP-3 and DIP-1 dipole surfaces shows that changing the sign of the isotropic dispersion term causes not only a decrease in the maximum peak intensity, but also significant changes in the relative intensities both within the central peak region of the spectrum and in its wings; in particular, a number of peaks in the wings nearly disappear.

5.2. *Simulations based upon a revised semi-empirical dipole moment surface*

We have seen that none of the above empirical modifications to the original dipole moment surface of [13] (surfaces DIP-1 to DIP-3 of table 3 and figure 6) truly succeeds in achieving good agreement between theory and experiment. In particular, compared to the experimental spectrum seen in figure 3, these simulations all show too much resolved structure in the intense peaks near the band origin. Comparison amongst these simulations suggests that it is the quadrupole and hexadecapole induction contributions to the dipole surface which determine the relative intensity pattern of this mid-IR spectrum. Our inability (to this point) to remove the structural complexity of the central peaks thus suggests that the values of the parameters for these dominant long-range induction terms are incorrect, and that further modifications to the dipole surface should focus on these terms.

The values for Q' and Φ' reported in table 2 of [13] (if taken at face value) appear to differ markedly from the *ab initio* values of Amos [22]. However, once the radial factor $\langle 1|\Delta r|0\rangle$ is taken into account, the only real discrepancy is in the sign of the hexadecapole radial derivative Φ'. Such a sign difference between the two major induction contributions to the dipole surface should lead to rather different contributions to the simulated spectrum, because cross-terms in the expression for the dipole moment give rise to interference effects in the calculated line intensities.

To investigate such effects, a simulation was carried out using a model dipole moment surface (DIP-4) in which all empirical terms were set to zero and the factors defining the induction terms [$Q'(N_2)$, $\Phi'(N_2)$ and α(Ar)] were fixed at their *ab initio* values (see table 3) [19, 22]. Figure 7 shows that this dipole function gives a mid-IR spectrum which is in much closer agreement with experiment than those obtained using the DIP-1 to DIP-3 model dipole surfaces; in particular, most of the unwanted structure in the strong central peaks has now disappeared. The spectrum simulated with DIP-4 is clearly in much better agreement with experiment than are any of those obtained using DIP-0 through DIP-3, both in the wings and in the region of the central peaks. Indeed, the DIP-4 simulation represents the major features of the experimental spectrum better than do any previous simulations for the N_2–Ar complex.

The relative sign of the quadrupole and hexadecapole derivatives Q' and Φ' clearly plays an important role in determining both the overall intensity of the simulated mid-IR spectrum and the pattern in the central region near the band origin. Comparison of the spectra simulated with the DIP-2 and DIP-4 dipole surfaces illustrates these points. The DIP-2 spectrum of figure 6 shows two strong peaks on both the left and right of the band origin, while the DIP-4 spectrum (uppermost curve in figure 7) shows only one strong peak on each side. This portion of the mid-IR spectrum is rather

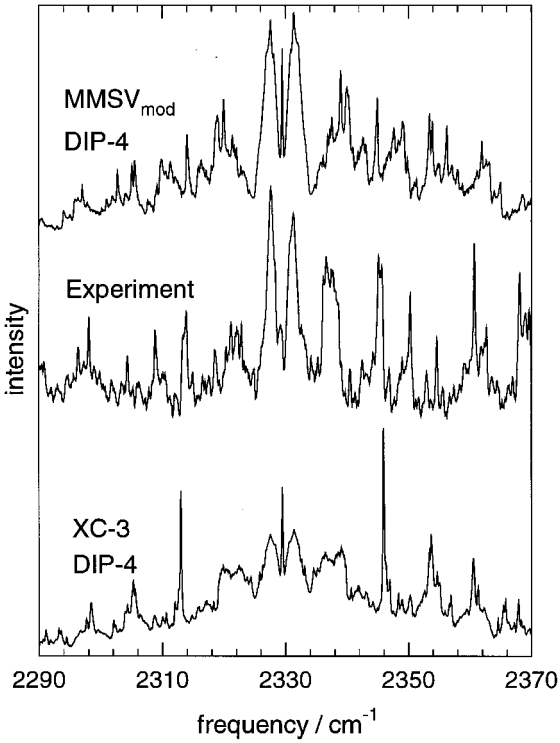

Figure 7. Comparisons with experiment [11] of simulated mid-IR spectra for 77 K obtained on combining the DIP-4 model dipole moment surface with the MMSV$_{mod}$ and XC-3 potential energy surfaces.

congested, containing a large number of individual transitions (about one-seventh of the total): the difference in sign between Q' and Φ' in the DIP-4 model dipole surface has presumably led to substantial changes of intensity in many of the transitions contributing to the strong central peaks appearing in the DIP-2 spectrum. The net result is that the four strong peaks obtained in the DIP-2 simulation are merged into the two broader, but still relatively strong central peaks appearing in the DIP-4 spectrum.

5.3. *Simulations based upon the XC-3 potential energy surface*

A good potential energy surface should lead to good IR spectra if a reliable dipole surface is available. We have therefore calculated the mid-IR spectrum for the N_2–Ar complex using the very recent XC-3 potential surface [8] and the improved DIP-4 model dipole moment surface discussed above. It was anticipated that the XC-3 potential surface might produce a better IR spectrum than does the MMSV$_{mod}$ surface, as it gives better agreement with most available bulk gas experimental data such as virial, binary diffusion and shear viscosity coefficients. It also gives excellent agreement with the experimental microwave frequencies reported for the various N_2–Ar isotopomers [7, 8]. This level of agreement with experiment indicates both that the XC-3 potential surface has a reliable isotropic component, and that the anisotropy of the bottom of the potential well is accurately represented [8].

Figure 7 compares the simulated mid-IR spectra obtained using the XC-3 and

$MMSV_{mod}$ potential surfaces with the experimental mid-IR spectrum [11]. Despite their apparent similarities (see figure 1), these two potential surfaces give quite different simulated mid-IR spectra, with that for the XC-3 potential surface differing much more from McKellar's experimental spectrum [11]. Thus, the XC-3 potential does not give as good a representation of the mid-IR spectrum as it does of the bulk gas experimental data and the microwave spectrum. It may therefore be concluded that while other experimental data are necessary, they are not sufficient to guarantee a completely accurate potential energy surface. The mid-IR spectrum provides detailed information on the potential energy surface both at the bottom of the well and on the repulsive wall of the surface up to the dissociation limit. The $MMSV_{mod}$ surface gives a better simulation of the experimental mid-IR spectrum than does the XC-3 surface when the same effective dipole moment surface (DIP-4) is employed; this implies that the well of the $MMSV_{mod}$ potential is more accurate than that of the XC-3 surface.

6. Prediction for the far-infrared spectrum

Although no experimental far-IR spectrum of the N_2–Ar complex has yet been published, its calculation is not without interest. The effective dipole moment function governing this part of the infrared spectrum is obtained by averaging over, rather than differentiating with respect to, the N_2 stretch coordinate to obtain the dispersion coefficient D_7^{00} and the permanent moments Q^{00} and Φ^{00} of equations (1) and (2). In a far-IR simulation for the $(N_2)_2$ complex, it was found that in the continuum (or collision-induced) infrared spectrum, overlap contributions to the dipole moment surface reduced the quadrupole contribution to the intensity through interference by about 10% [15], while the pure hexadecapole and overlap contributions to the gas-phase spectrum were 5% and 1%, respectively [28]. Indeed, a more detailed dipole model could, in principle, be inferred from the intensity patterns within the experimental far-IR spectrum [15], although this would not be an easy task, even if a fully-resolved spectrum were available.

Brocks and van der Avoird showed that the line strengths for the more intense $(N_2)_2$ far-IR spectrum can be calculated to within a factor two by using only the long-range multipole–induction terms [15]. Our simulation of the far-IR spectrum of N_2–Ar has therefore been based upon approximating the dipole surface of the complex by the long-range induction contributions. This is equivalent to using DIP-4 with the factors $Q'\langle 1|\Delta r|0\rangle$ and $\Phi'\langle 1|\Delta r|0\rangle$ replaced by the vibrationally-averaged quantities Q^{00} and Φ^{00} (i.e. to employing equations (1) and (2) with $D_7^{00} = 0$). The experimental values of Q^{00} and Φ^{00} listed in table 4 were therefore combined with the *ab initio* value of α(Ar) to define the dipole surface used for this simulation.

The simulation of the far-IR spectrum included all allowed transitions between truly bound vibration–rotation states, starting from the ground state and ending at the first allowed dissociation channels for the ground or the first excited rotational states of the $^{14}N_2$ monomer, subject to the selection rules of equations (5) and (6). This leads to more than 5×10^4 individual transitions within the frequency range $0 < \nu_{if}^{\text{far-IR}} \leqslant 85{\cdot}3\ \text{cm}^{-1}$. The resulting simulated far-IR spectra obtained at 5 K and 77 K using the $MMSV_{mod}$ potential surface are shown in figure 8. For the 5 K spectrum, a Lorentzian lineshape with a linewidth of $0{\cdot}04\ \text{cm}^{-1}$ has been assumed for each transition (following [15]), and Q-, P- and R-branch assignments are shown for the most intense peaks. A Lorentzian lineshape function with a $0{\cdot}20\ \text{cm}^{-1}$ linewidth [13, 15] has been employed in generating the 77 K spectrum.

Table 4. Dipole moment parameters used in the present work and in [13].

Parameters	Present work Value	Present work Source	Previous work [13]
$Q'/e\,a_0$	1·15	[22]	1·15
$\Phi'/e\,a_0^3$	−2·53	[22]	2·52
$Q^{00}/e\,a_0^2$	−1·09	[28]	–
$\Phi^{00}/e\,a_0^4$	−10·4	[28]	–
$\alpha/e\,a_0^3$	11·062	[19]	11·075

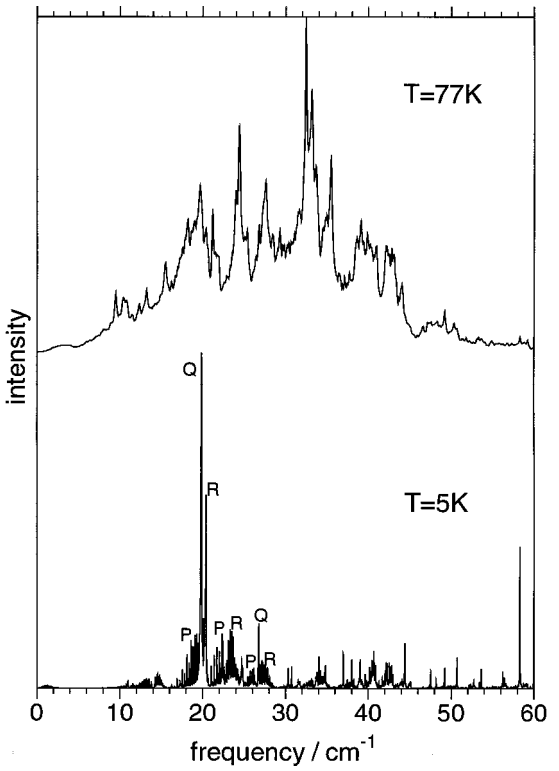

Figure 8. Simulated far-IR spectra generated from the $MMSV_{mod}$ potential and the pure induction dipole surface of equations (1) and (2) and table 4 (with $D_7^{00} = 0$); individual lines were assigned Lorentzian linewidths of 0·04 and 0·20 cm^{-1} at 5 and 77 K, respectively.

As indicated by Tennyson *et al.* [27], the effort involved in carrying out these spectral calculations can be reduced significantly by introducing a cut-off criterion such that only transitions having intensities greater than (say) 0·1% of the most intense line are used in synthesizing the spectrum. For the mid-IR spectrum this was shown to cause unacceptable changes in the predicted spectrum near the band centre. However, in the far-IR simulations the factor $F(\nu_{if}, T)$ (see equation (8)) strongly suppresses all low-frequency transitions: e.g., for transitions lying at frequencies of 0·1, 1·0 and 10·0 cm^{-1}, respectively, $F(\nu_{if}, T) = 1{\cdot}86 \times 10^{-4}$, $1{\cdot}85 \times 10^{-2}$ and 1·70 cm^{-1}. As a result, although the 0·1% cut-off criterion deletes nearly half of all possible

transitions, it causes no obvious changes in the resulting predicted far-IR spectrum: indeed, utilization of this criterion merely reduces the overall intensities of the spectra seen in figure 8 by about 0·1%. Hence, while quite *in*appropriate for mid-IR spectra, the 0·1% intensity cut-off criterion can be used satisfactorily in the simulation of far-IR spectra.

It is interesting to note that these predicted far-IR spectra for the N_2–Ar complex at 5 K and 77 K have patterns more akin to those simulated by Brocks and van der Avoird [15] for the $(N_2)_2$ complex at 2 K and 25 K, respectively, than to those simulated by Ayllón *et al.* [13] for the N_2–Ar complex at 5 K and 77 K. This is particularly obvious at 77 K. For example, a strong peak near 19 cm^{-1} in our 77 K spectrum has an intensity that is 50% of that of the strongest peak (at 32 cm^{-1}), whereas in [13] this same peak has an intensity that is 80% of the strongest peak (also at 32 cm^{-1}). Moreover, some weak peaks around 46–51 cm^{-1} with intensities that are 10% of that of the strongest peak did not appear in the earlier simulation [13]. This is certainly due in part to the employment of different potential surfaces in the two simulations: however, this is unlikely to explain all differences between the two sets of results, as the potential surface [15] for the N_2–N_2 complex certainly differs even more from either of the two N_2–Ar potential surfaces than they do from one another.

A more likely source of such differences lies in the model dipole moment surfaces used in the simulations. Both the current N_2–Ar calculations and those of Brocks and van der Avoird [15] for $(N_2)_2$ employed only the quadrupole and hexadecapole induced-dipole contributions to the corresponding dipole surfaces. In contrast, the dipole surface of Ayllón *et al.* [13] also included the dispersion and short-range (exponential) overlap contributions seen in equations (9) and (10). In [13] the parameters D_{01}^{00}, D_{23}^{00}, D_7^{00}, Q^{00} and Φ^{00} characterizing the far-IR dipole surface were all assumed to be about 20-times larger than the corresponding derivatives (given in table 3) characterizing the mid-IR dipole surface DIP-0. Since only *relative* intensities were presented for the far-IR spectra, the (common) scale factor will be cancelled out, with the consequence that the far-IR simulations of [13] appear, in effect, to be based upon the same dipole derivative surface that was employed for the mid-IR spectral simulation. However, table 4 shows that the ratio Φ^{00}/Q^{00} is actually quite different from Φ'/Q', so the resulting spectra should be expected to be quite different.

At the time of writing, no experimental data had been published for the far-IR spectra of either the N_2–N_2 or the N_2–Ar complex. Measurements of the far-IR absorption spectrum of N_2–Ar mixtures have now been made by Wishnow [29, 30], but a full analysis was not available prior to completion of this work, so that comparisons with the present calculations were not possible.

7. Conclusions and discussion

Mid-infrared spectra of the $^{14}N_2$–Ar van der Waals complex have been simulated for a temperature of 77 K and an assumed Lorentzian linewidth of 0·2 cm^{-1}, which are consistent with the experimental conditions of McKeller [11], using the recently published $MMSV_{mod}$ and XC-3 potential surfaces together with various model dipole moment surfaces. The calculations include all truly bound states of the complex, which has total rotational angular momentum quantum number up to and including $J = 34$. Over 10^5 transitions among some 2000 bound states have been included in each of these simulations. The spectrum obtained using the $MMSV_{mod}$ potential and a new model dipole surface gives better agreement with experiment than do those synthesized

by us using the XC-3 potential or by Ayllón *et al.* [13] using the earlier CPV potential. This implies that the attractive well of the $MMSV_{mod}$ potential energy surface is more realistic than those of other proposed potentials for this system. We have also found that the dipole surface proposed by Ayllón *et al.* [13] is not appropriate, and that use of an intensity cut-off criterion introduces substantial errors into simulations of the mid-IR spectrum.

The dipole surface utilized by Ayllón *et al.* [13] in their simulations using the CPV potential surface [3] included both short-range overlap/exchange and isotropic long-range dispersion contributions, in addition to induction contributions [15]. An isotropic dispersion term was introduced [13] in order to suppress the intense Q-branch peak at the band centre ν_0, while short-range contributions were introduced to enhance the peaks near $\nu_0 \pm 3$ cm^{-1}. We have found that, when the signs of Q' and Φ' are (incorrectly) taken to be the same (as appears to be the case in [13]), the isotropic dispersion contribution plays a fairly significant role in determining the relative intensities in the mid-IR spectrum, and is effective in suppressing the so-called zero-frequency spike at the very centre of the spectrum. However, when Q' and Φ' have opposite signs, as is the case for the *ab initio* values defining the present DIP-4 dipole surface [22], the role of the isotropic dispersion term is much reduced, and in a sense reversed: in particular, the central spike becomes *less* intense when D_7' is set to zero. The differences between these two sets of results must be associated with the relative amounts of constructive and destructive interference arising from the interplay between the two induction terms and the isotropic dispersion term. As the main role of the short-range contributions to the dipole surface is to enhance the overall intensity of the simulated mid-IR spectrum, and as these terms appear to have only a small effect on the *relative* intensities of the various peaks, it may be difficult to say very much about their importance until experimental absolute intensities become available.

Far-IR spectra at 5 K and 77 K have also been simulated using the $MMSV_{mod}$ potential surface and an appropriate dipole surface. The final model dipole surfaces proposed here for far- and mid-IR spectral simulations both retain only the long-range induction contributions and differ solely in their parameterizations, namely the vibrationally averaged quantities Q^{00} and Φ^{00} are used in the far-IR simulations while the derivatives Q' and Φ' govern the mid-IR simulations. An intensity cut-off criterion plays a different role in generating the far-IR spectrum than it does in generating the mid-IR spectrum of the complex. In the far-IR region, frequency and population factors strongly suppress the intensities of the very large numbers of weak transitions lying near the band origin so, *unlike* the mid-IR case, the employment of an intensity cut-off criterion has little effect on the predicted spectrum.

One shortcoming of the present study is the fact that (following Ayllón *et al.* [13]) the calculations considered only discrete transitions among the truly bound states of N_2–Ar. Both relative population arguments and the calculations of Brocks [17] show that transitions involving metastable rotationally predissociating states contribute considerably to the infrared spectra, especially at frequencies far from the band centres. However, the moderately large linewidths (of ca. 1 cm^{-1}) predicted for such levels [17] means that they will contribute little to the character of the fine structure of these spectra, and hence will not provide very quantitative tests of the accuracy of different potential energy surfaces. Thus, while our neglect of such states artificially reduces the overall intensities of the predicted spectra, especially at frequencies far (say $\geqslant 40$ cm^{-1}) from the band centres, it should have little effect on our conclusions regarding the quality of various potential energy and dipole moment surfaces.

This work has been supported by the Natural Sciences and Engineering Research Council (NSERC) of Canada through grants in aid of research to F.R.W.M. and R.J.L., and through the award of an NSERC International Post-doctoral Fellowship to F.W. We are pleased to acknowledge helpful discussions with Dr C. Bissonnette, and to thank Mr E. E. Hanson for computer technical support. We also thank Dr A. R. W. McKellar for providing the digital representations of his 77 K spectrum and for bringing the far-IR work of Wishnow to our attention, and Dr J. Tennyson for providing us with the TRIATOM suite of programs. We are also pleased to acknowledge helpful discussions with Professor M. S. Child and Dr J. M. Hutson.

References

[1] Pattengill, M. D., La Budde, R. A., Bernstein, R. B., and Curtiss, C. F., 1971, *J. chem. Phys.*, **53**, 5517.
[2] Rotzoll, G., 1982, *Chem. Phys. Lett.*, **88**, 179.
[3] Candori, R., Pirani, F., and Vecchiocattivi, F., 1983, *Chem. Phys. Lett.*, **102**, 412.
[4] Bowers, M. S., Tang, K. T., and Toennies, J. P., 1988, *J. chem. Phys.*, **88**, 5465.
[5] Gianturco, F. A., Venanzi, M., and Dickinson, A. S., 1990, *J. chem. Phys.*, **93**, 5552.
[6] Beneventi, L., Casavecchia, P., Volpi, G. G., Wong, C. C. K., and McCourt, F. R. W., 1993, *J. chem. Phys.*, **98**, 7926.
[7] Jäger, W., Gerry, M. C. L., Bissonnette, C., and McCourt, F. R. W., 1994, *Faraday Discuss., chem. Soc.*, **97**, 105.
[8] Dham, A. K., McCourt, F. R. W., and Meath, W. J., 1995, *J. chem. Phys.*, **103**, 8447.
[9] Jäger, W., and Gerry, M. C. L., 1992, *Chem. Phys. Lett.*, **196**, 274.
[10] Henderson, G., and Ewing, G. E., 1974, *Molec. Phys.*, **27**, 903.
[11] McKellar, A. R. W., 1988, *J. chem. Phys.*, **88**, 4190.
[12] Dunker, A. M., and Gordon, R. G., 1978, *J. chem. Phys.*, **68**, 700.
[13] Ayllón, A. G., Santamaría, J., Miller, S., and Tennyson, J., 1990, *Molec. Phys.*, **71**, 1043.
[14] Beswick, J. A., and Shapiro, M., 1982, *Chem. Phys.*, **64**, 333.
[15] Brocks, G., and van der Avoird, A., 1985, *Molec. Phys.*, **55**, 11.
[16] Brocks, G., and van der Avoird, A., 1987, in *Structure and Dynamics of Weakly Bound Molecular Complexes*, edited by A. Weber (NATO ARW series) (Dordrecht: Reidel), pp. 337–355.
[17] Brocks, G., 1988, *J. chem. Phys.*, **88**, 578.
[18] Chuaqui, C. E., Le Roy, R. J., and McKellar, A. R. W., 1994, *J. chem. Phys.*, **39**, 101.
[19] Hettema, H., Wormer, P. E. S., and Thakkar, A. J., 1993, *Molec. Phys.*, **80**, 533.
[20] Mills, I., Cvitaš, T., Homann, K., Kallay, N., and Kuchitsu, K., 1993, *Quantities, Units and Symbols in Physical Chemistry*, 2nd edn. (Oxford: Blackwell).
[21] Hutson, J. M., 1991, in *Advances in Molecular Vibrations and Collision Dynamics*, edited by J. M. Bowman (Greenwich, CT: JAI Press), Vol. 1A, pp. 1–45.
[22] Amos, R. D., 1980, *Molec. Phys.*, **39**, 1.
[23] Huber, K. P., and Herzberg, G., 1979, *Molecular Spectra and Molecular Structure. IV. Constants of Diatomic Molecules* (New York: Van Nostrand Reinhold).
[24] Bernath, P. F., 1995, *Spectra of Atoms and Molecules* (Oxford: Oxford University Press).
[25] Tennyson, J., Miller, S., and Le Sueuer, C. R., 1993, *Comput. Phys. Commun.*, **75**, 339.
[26] Bendtsen, J., 1974, *J. Raman Spectrosc.*, **2**, 133.
[27] Tennyson, J., Miller, S., and Henderson, J. R., 1992, in *Computational Chemistry*, edited by S. Wilson (New York: Plenum), Vol. 4, pp. 91–144.
[28] Poll, J. D., and Hunt, J. L., 1981, *Can. J. Phys.*, **59**, 1448.
[29] Wishnow, E. H., 1993, Ph.D. thesis, University of British Columbia.
[30] Wishnow, E. H., Gush, H. P., and Ozier, I., 1996, *J. chem. Phys.*, **104**, 3511.